Free surface flow simulation with application to bluff body flow control

Serpil Kocabiyik[1] **and Canan Bozkaya**[2]

[1]Memorial University of Newfoundland
St. John's, NL, Canada

[2]Middle East Technical University
Ankara, Turkey

- To better understand the interaction of a free surface wave motion with moving bodies, two-dimensional flow of a viscous incompressible fluid past an oscillating cylinder beneath a free surface is investigated numerically.
- Such flows are found in ocean engineering applications and undersea technology.

- The transformation between kinetic and potential energies and the coexistence of viscous and gravity forces at an unknown wavy boundary make the free surface phenomena difficult to study.
- The interaction of a free surface with bluff body wakes has been principally the subject of experimental studies, see for example:

- Cetiner and Rockwell (2001)
  J. Fluid Mech., Vol.427:29-59
- Sheridan, Lin and Rockwell (1997)
  J. Fluid Mech., Vol.330:1-30

- Computations of nonlinear viscous free surface problems including cylindrical bodies are relatively few, see for example:

- Reichl, Hourigan and Thompson (2005)
  J. Fluid Mech., Vol.533:269-296
- Bozkaya, Kocabiyik, Mironova, Gubanov (2011)
  J. Comput. Appl. Math., Vol.235:4780-4795

Uniform flow past a stationary cylinder

- Oppositely signed vortices shed alternatively at either side of the cylinder at f_0^* to form the von Kármán vortex street ($R \geqslant 40$).
- Natural shedding frequency frequecy: $f_0 = df_0^*/U$.
  Reynolds number: $R = dU/\nu$
- Vortex shedding exerts a periodic resultant force on the body:
  x-component: drag force frequency $\sim 2f_0$; y-component: lift force frequency $\sim f_0$.

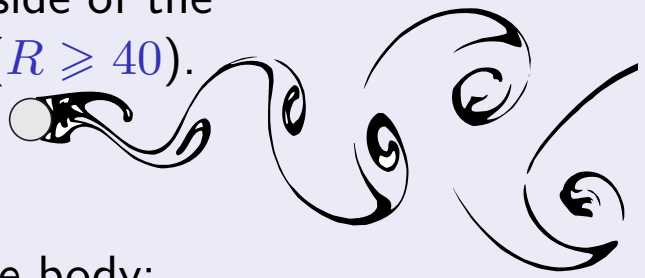

Uniform flow past a cylinder under forced oscillations

- Wake structure strongly depends on the amplitude A and (f/f_0)
- Resonance of cylinder vibration and vortex shedding frequencies is known as lock-on

(for transverse or rotational oscillations: $f \sim f_0$, for streamwise oscillations: $f \sim 2f_0$.)

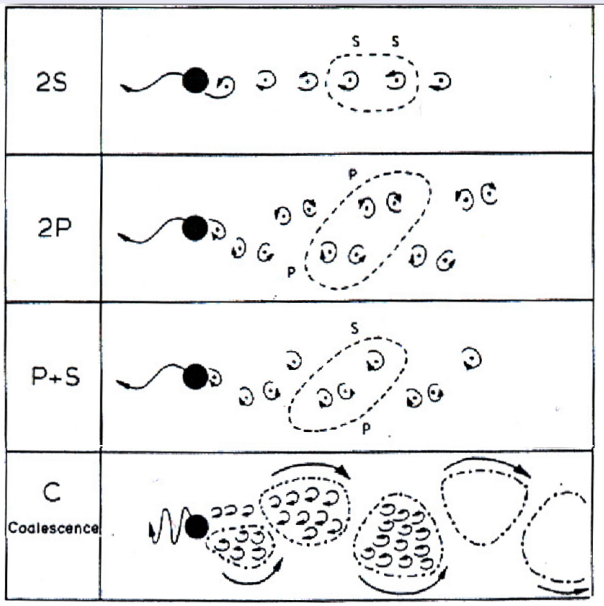

Vortex locked-on modes near the fundamental lock-on region.

Williamson and Roshko (1988) *J. Fluid Struct.* Vol. 2: 355-381
(transverse osc.: $300 \leqslant R \leqslant 10^3$, $0.2 \leqslant A \leqslant 1.8$, $f/f_0 \geqslant 0.3$)

- Each mode is defined by the number of pairs, "**P**", and single vortices, "**S**", shed per T_v
  T_v: a single vortex shedding cycle, $T_v = kT$, k=fraction or integer

2S: two single vortices of opposite sign are shed per T_v (the classical von Kármán street);
2P: two counter-rotating pairs are shed per T_v;
P+S: one single and a pair of co-rotating vortices are shed per T_v;
C: coalescence of vortices either immediately behind or in the downstream of the cylinder

Flow configuration

The cylinder is forced to oscillate at a prescribed amplitude, A^*, and forcing frequency, f^*, in the streamwise direction

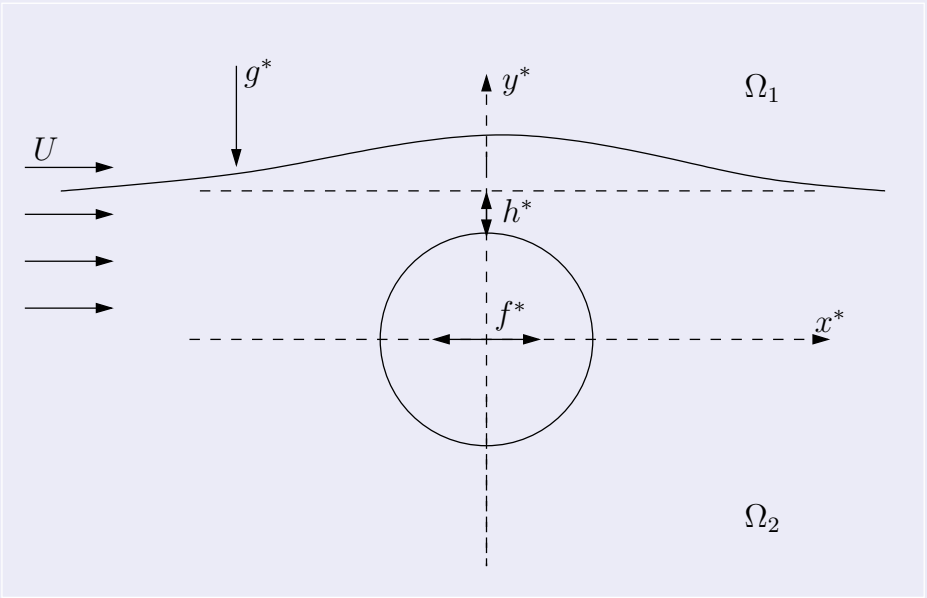

g^*: acceleration due to gravity
d: cylinder diameter
U: free stream velocity
h^*: submergence depth
$x^*(t^*)$: cylinder displacement

Harmonic oscillations of the cylinder:
$x^*(t^*) = A^* \cos(2\pi f^* t^*)$

Fluid properties:
$\rho_1/\rho_2 = 1/100, \quad \nu_1/\nu_2 = 1$
(Reichl, Hourigan and Thompson (2005), *J. Fluid Mech., Vol.533:269-296*)

Dimensionless flow parameters

$R = Ud/\nu_2$: Reynolds number (ν: kinematic viscosity coefficient)
$Fr = U/\sqrt{dg^*}$: Froude number
$h = h^*/d$: depth of cylinder submergence
$A = A^*/d$: forcing amplitude of cylinder
$f/f_0 (= f^*/f_0^*)$: forcing-to-natural shedding frequency ratio($f_0 = df_0^*/U$ and $f = df^*/U$)

$t = Ut^*/d$: : dimensionless time
$p/\varepsilon = p^*/\rho_2 U^2$: pressure

$$\varepsilon = \begin{cases} \rho_1/\rho_2 & \text{in } \Omega_1, \\ 1 & \text{in } \Omega_2. \end{cases}$$

Integral form of 2D unsteady governing equations:

$$\frac{d\mathbb{V}}{dt} + \int_{\mathbb{A}} (\vec{u} \cdot \vec{n}) \, \mathrm{d}S = 0$$

$$\frac{d}{dt} \int_{\mathbb{V}} \vec{u} \, \mathrm{d}V + \int_{\mathbb{A}} (\vec{n} \cdot \vec{u}) \vec{u} \, \mathrm{d}S = -\frac{1}{\varepsilon} \int_{\mathbb{A} \cup \mathbb{I}} p \vec{n} \, \mathrm{d}S + \frac{1}{R} \int_{\mathbb{A} \cup \mathbb{I}} \vec{n} \cdot \nabla \vec{u} \, \mathrm{d}S + \int_{\mathbb{V}} \vec{F} \, \mathrm{d}V$$

$$\vec{F} = (-a_1, \; 1/Fr^2 - a_2, \; 0)$$

$\vec{a}=(a_1, a_2, 0)$: acceleration of the non-inertial frame of reference

$\vec{u}=(u, v, 0)$: velocity vector

$\vec{n}$: outward normal vector

$\mathbb{V}$: fractional volume open to flow

$\mathbb{A}$: fractional area open to flow

$\mathbb{I}$: fluid-body interface

Boundary conditions:

- cylinder boundary: $u = 0, \; v = 0$
- top/bottom boundaries: $\dfrac{\partial u}{\partial x} = 0, \; v = -v_2$
- inflow: $u = 1 - v_1, \; v = -v_2$
- outflow: $\dfrac{1}{R}\dfrac{\partial u}{\partial x} + \dfrac{\bar{h}}{Fr^2} = p, \; \dfrac{\partial v}{\partial x} = 0$

$(v_1, v_2, 0)$: velocity of the non-inertial frame of reference, $\bar{h}$: height of the fluid at the outflow

Initial conditions:

- $t = 0$: uniform flow, i.e., $u(x, y, 0) = 1 - v_1, \quad v(x, y, 0) = -v_2$
- Free surface at $t = 0$ is assumed to be undisturbed.

- Finite volume discretization is used on a fixed non-boundary fitted Cartesian grid
- Displacement of the free surface is captured by using the volume of fluid method (Hirt and Nichols (1981), *J. Comp. Phys.*, Vol.39:201-225)
- Free surface advection is performed by the strictly mass conserving volume of fluid advection method in two-dimensional incompressible flows (Aulisa, Manservisi, Scardovelli (2003), *J. Comp. Phys.* Vol.192:355-364)
- Fluid-body interface is discretized using the fractional area/volume obstacle representation method (Hirt and Sicilian (1985), *Flow Science, Inc., New Mexico*) and the cut cell method (Gerrits (2001), *Ph.D. Thesis, University Groningen*)
- A second order accurate central-difference scheme is used to discretize the governing equations. A cell merging procedure is used to preserve a global second-order accuracy of the spatial discretization.
- A coupled sparse linear system in primitive variables is solved using a generalized minimal residual method to determine the discretized pressure and velocity fields corresponding to the successive time instants.
- First-order explicit forward Euler scheme is used to advance the solution in time.
- The simulations are carried out using the CFD code developed by S. Kocabiyik's research group at Memorial University.

VOF
fs advection
favor
continuity-NS
matrix-structure
Simulation Workflow

Volume of fluid (VOF) method Hirt and Nichols (1981) *J. Comp. Phys.*, Vol.39:201-225

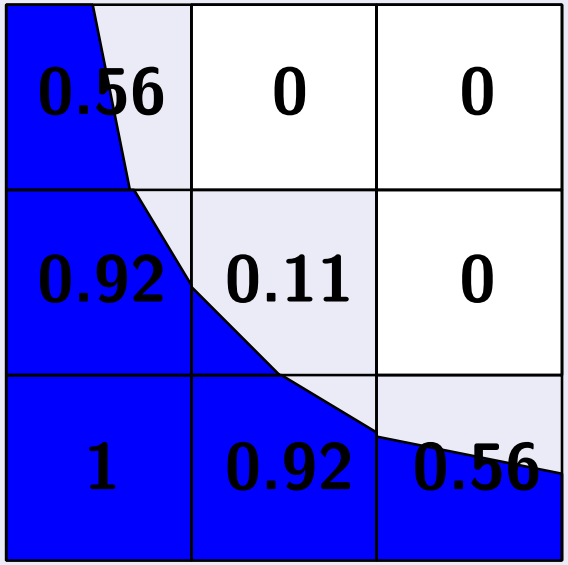

1. Free surface interface is reconstructed using VOF function $0 \leq F_{f,i,j} \leq 1$ which defines cells that are empty, full, or partially filled with fluid, f in Ω_2:

   $F_{f,i,j}$: the fractional volume of a computational cell that is occupied by the fluid (i.e., the ratio of the fluid in each cell)

   Interface within each mixed cell is approximated with a straight line segment

   - Interface normal is estimated using fluid fractions in adjacent cells
   - Interface line is uniquely defined by its normal and fluid fraction in its cell

   fs reconstruction

2. The fluid region is advected in time to its new position with the velocity field:
   the new values of $F^{n+1}_{f,i,j}$ are computed in all computational cells based on the old values, $F^{n}_{f,i,j}$, and $\vec{u}^n = (u^n, v^n, 0)$

   fs advection

Advantages of the VOF method

- This method can define sharp interfaces and is robust
- Interface topology changes handled automatically
- Low memory and computational cost
- Implemented in CFD software FLUENT and FLOW3D

Method

- A Cartesian non-boundary fitted Eulerian grid is used.
- A finite volume discretization is applied to computational cells (control volumes) which are built around discrete grid knots.

Staggered grid representation

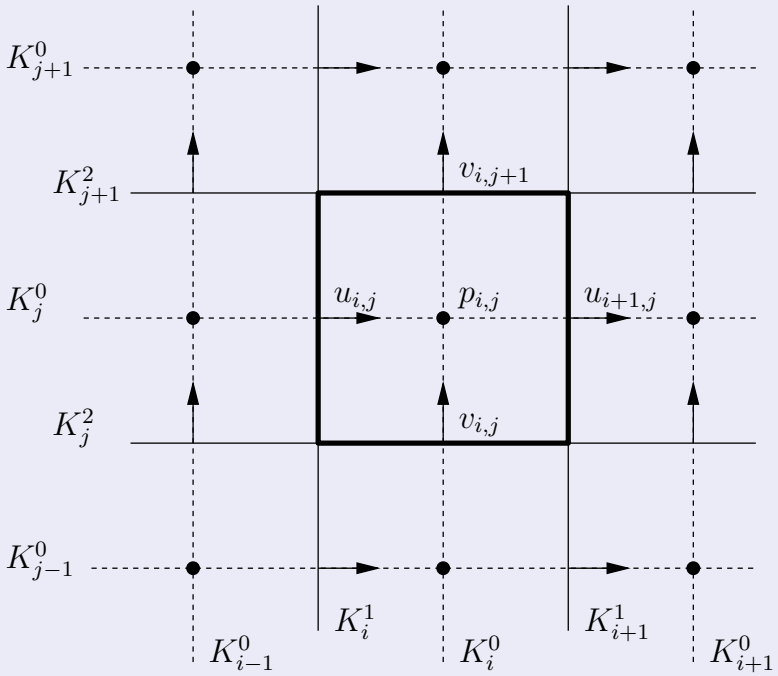

- The staggered grid involves three different sets of knots: $p_{i,j}$, $u_{i,j}$, $v_{i,j}$
- Velocity knots are located on the edges of computational cells corresponding to pressure knots

continuity equation cell: $(K^1_i, K^2_j) - (K^1_{i+1}, K^2_{j+1})$

x-momentum equation cell: $(K^0_{i-1}, K^2_j) - (K^0_i, K^2_{j+1})$

y-momentum equation cell: $(K^1_i, K^0_{j-1}) - (K^1_{i+1}, K^0_j)$

Time discretization

First-order explicit forward Euler scheme

$$\int_{t^n}^{t^n+\Delta t} I \, \mathrm{d}t = \Delta t I(t^{n+1})$$

n: iteration counter

$\Delta t = t^{n+1} - t^n$: time step

◀ Method

- Cell labeling is used to distinguish cells in which (i) the governing equations are solved and (ii) the boundary conditions are satisfied
- Each pressure cell is labeled based on a value of fractional volume open to flow, $\mathbb{V}/V$, in this cell
- Edge of pressure cell on which u- or v-velocity knot is located (velocity cell) is labeled according to the types of pressure cells this edge belongs to

◂ Method

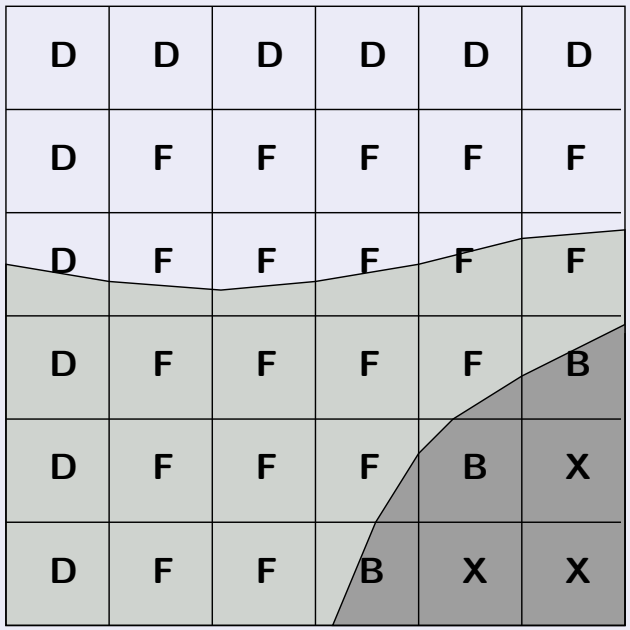

Pressure cells labels

F(luid):	Cells for which $\mathbb{V}/V \geqslant 0.5$
B(oundary):	Fluid-body interface cells
D(omain):	Computational domain boundary cells
(e)**X**(cluded):	Cells occupied by the body

- Continuity equation is discretized in all the **F** cells
- Value of pressure is set to zero in **B**, **D** and **X** knots

Velocity cells labels

FF, **BF**, **BX**, **DF**, **BB**, **DD**, **XX**

- Navier-Stokes equations are discretized in all the **FF** cells
- Values of velocities **BF**, **BB**, **BX** and **XX** are set to zeros
- **DF** and **DD** velocities are used to apply boundary conditions at the computational domain boundary

- When the cylinder moves through the fixed staggered grid, the pressure cell which belongs to the cylinder at time $t = t^n$ may become the fluid cell at time $t = t^{n+1}$. The continuity equation needs to be discretized in this pressure cell.
- Since at time $t = t^n$ the velocities in the pressure cell do not satisfy the mass balance exactly, the pressure field has to do extra work to restore the mass balance in the pressure cell at time $t = t^{n+1}$. This extra work seems to reflect as a spike in the pressure:

Fekken (2004) and Kleefsman (2005) [PhD Thesis, University of Groningen]

- The pressure spikes are eliminated by using a non-inertial frame of reference:

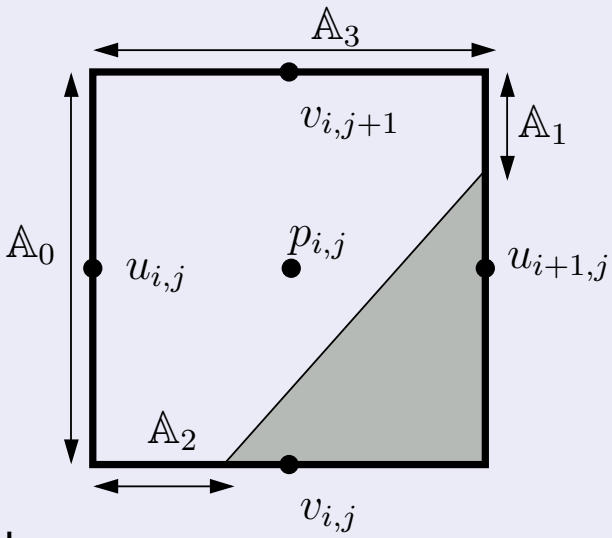

$$\frac{d\mathbb{V}}{dt} + \int_{\mathbb{A}} (\vec{n} \cdot \vec{u}) \, \mathrm{d}S = 0$$

- In non-inertial frame of reference $\dfrac{d\mathbb{V}_{p_{i,j}}}{dt} = 0$
- Convective term is approximated as a sum of convective fluxes, $f_{\mathbb{A}_k}$, through each edge aperture

$$\int_{\mathbb{A}} \vec{n} \cdot \vec{u} \, \mathrm{d}S = \sum_{k=0}^{3} f_{\mathbb{A}_k}, \qquad f_{\mathbb{A}_k} = \int_{\mathbb{A}_k} \vec{n} \cdot \vec{u} \, \mathrm{d}S$$

where

$$f_{\mathbb{A}_0} = -\left(u_{i,j}\mathbb{A}_0\right)^{n+1}, \quad f_{\mathbb{A}_1} = \left(u_{i+1,j}\mathbb{A}_1\right)^{n+1}, f_{\mathbb{A}_2} = -\left(v_{i,j}\mathbb{A}_2\right)^{n+1}, \quad f_{\mathbb{A}_3} = \left(v_{i,j+1}\mathbb{A}_3\right)^{n+1}$$

The resulting linear equation

Method

$$-\left(u_{i,j}\mathbb{A}_0\right)^{n+1} + \left(u_{i+1,j}\mathbb{A}_1\right)^{n+1} - \left(v_{i,j}\mathbb{A}_2\right)^{n+1} + \left(v_{i,j+1}\mathbb{A}_3\right)^{n+1} = 0$$

$$\frac{d}{dt}\int_{\mathbb{V}} u \, \mathrm{d}V + \int_{\mathbb{A}} (\vec{n}\cdot\vec{u})u \, \mathrm{d}S = -\frac{1}{\varepsilon}\int_{\mathbb{A}\cup\mathbb{I}} pn_1 \, dS + \frac{1}{R}\int_{\mathbb{A}\cup\mathbb{I}} \vec{n}\cdot\nabla u \, dS + \int_{\mathbb{V}} F_1 \, dV$$

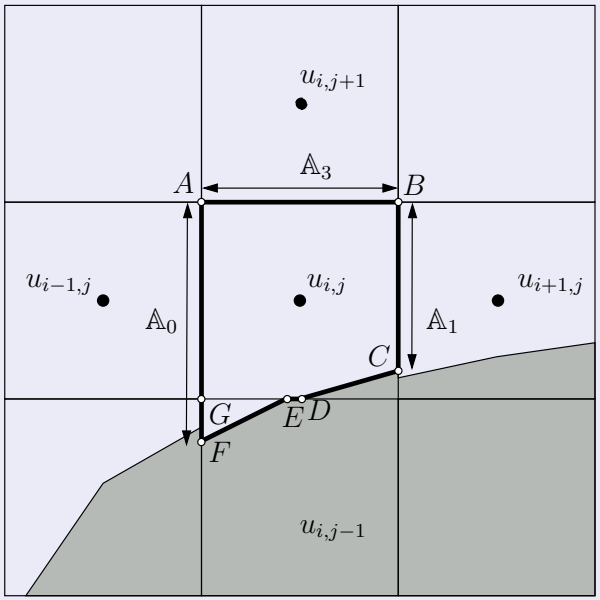

- **FF** cell borders **FF**, **DF** or **DD** cell
  Velocities and their normal derivatives at the edges of velocity cells are approximated using a linear interpolation between fluid neighbour velocity knots (standard discretization)
- **FF** cell borders **BF** cell (neighbour velocity may be located in the region occupied by the solid body)
  1. Cell merging procedure is used
  2. Velocities and their normal derivatives at the edges of velocity cells are approximated separately for each edge of **FF** cell
  3. A second-order approximation to diffusive and convective fluxes is obtained using a two-dimensional B-spline interpolation

The resulting linear equation

Method

$$C_0 u_{i,j}^{n+1} + C_1 u_{i-1,j}^{n+1} + C_2 u_{i+1,j}^{n+1} + C_3 u_{i,j-1}^{n+1} + C_4 u_{i,j+1}^{n+1} + C_5 p_{i-1,j}^{n+1} + C_7 p_{i,j}^{n+1} = C_8$$

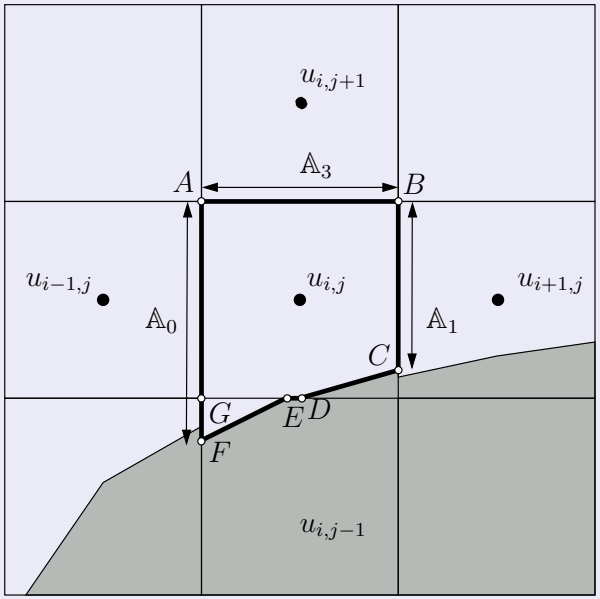

Time derivative is approximated using the midpoint rule as

$$\frac{d}{dt}\int_{\mathbb{V}} u \, \mathrm{d}V \approx \frac{d\left(u_{i,j}\mathbb{V}_{u_{i,j}}\right)}{dt}$$

where, in general,

$$\mathbb{V}_{u_{i,j}} = \mathbb{V}_{\mathbf{FF}} + \sum_{i=0}^{N'} \mathbb{V}_{\mathbf{BF}}, \qquad N' = 0, \ldots, 3.$$

N': number of slaves merged with the master cell, $\mathbb{V}_{\mathbf{FF}}$: volume aperture of the master cell, $\mathbb{V}_{\mathbf{BF}}$: volume aperture of the slave cell

In a situation shown in figure above,

- the master cell is cut by the cylinder geometry
- the cell has the only slave
- $\mathbb{V}_{u_{i,j}} = \mathbb{V}_{ABCDEG} + \mathbb{V}_{GEF}$

Thus,

$$\frac{d\left(u_{i,j}\mathbb{V}_{u_{i,j}}\right)}{dt} \approx \frac{u_{i,j}^{n+1}\mathbb{V}_{u_{i,j}}^{n+1} - u_{i,j}^{n}\mathbb{V}_{u_{i,j}}^{n}}{\Delta t},$$

- Free surface is defined in the computational cells where a rapid change in density, ρ, and viscosity, μ, occurs
- Density in the vicinity of the phase interface is computed as

$$\rho' = \frac{F_a^{n+1}\rho_1 + F_f^{n+1}\rho_2}{\bar{\mathbb{V}}^{n+1}}$$

F_a^{n+1} and F_f^{n+1}: fractions of the air and the fluid in the velocity cell

$\bar{\mathbb{V}}^{n+1}$: fractional volume aperture

- F_a^{n+1} is calculated from F_f^{n+1} and F_b^{n+1} as

$$F_a^{n+1} = 1 - (F_f^{n+1} + F_b^{n+1})$$

- Dimensionless counterpart of the averaged density, ρ', can be written as

$$\varepsilon^{n+1} = \frac{\rho'}{\rho_2} = \frac{\rho_1/\rho_2 F_a^{n+1} + F_f^{n+1}}{\bar{\mathbb{V}}^{n+1}}$$

- $F_a^{n+1} = 0$, $\varepsilon^{n+1} = 1$: momentum equation is discretized for the fluid phase
- $F_f^{n+1} = 0$, $\varepsilon^{n+1} = \rho_1/\rho_2$: momentum equation is discretized for the air phase

Piecewise linear interface (PLIC) algorithm

Free surface interface is approximated with a straight line segment:

$$\vec{n}\vec{x} + \bar{d} = 0,$$

$\vec{n}$: unit outward normal (points outward the fluid, f, in Ω_2); $\bar{d}$: the distance from origin

Computation of the normal vector, $\vec{n}$: Gerrits (2001), *Ph.D. Thesis, Univ. Groningen*

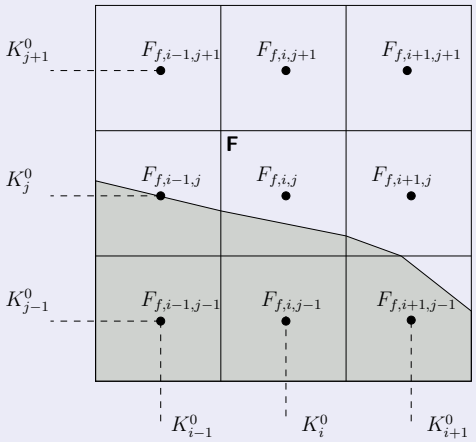

- Location of the free-surface interface is reconstructed from the local F_f data at any time in the solution
- $\vec{n}$ is determined by approximating:

$$\vec{n} = \nabla F_f$$

in each cell $p_{i,j}$ having $0 < F_{f,i,j} < 1$ with respect to eight neighbours surrounding the cell.

- The calculated normal vector, $\vec{n}$, is normalized: $\vec{n} = \frac{\nabla F_f}{|\nabla F_f|}$

Computation of the line distance, $\bar{d}$: Rider and Kothe (1998) *J. Comput. Phys., Vol.141:112-152*

- The value of $\bar{d}$ is constrained by mass conservation: resulting line passes through the computational cell with a truncation volume equal to the cell volume aperture, $\mathbb{V}$, so that

$$\mathbb{V}(\bar{d}) - \mathbb{V} = f(\bar{d})$$

$\mathbb{V}(\bar{d})$: truncation volume; $f(\bar{d})$: non-linear function

- Brent's root finding algorithm is used to compute $\bar{d}$:
  R.P. Brent (1973) *Algorithms for Minimization without Derivatives.*
  New Jersey: Prentice-Hall

◂ free surface interface capturing

Geometrical area preserving VOF advection method:

Aulisa, Scardovelli, Manservisi and Zaleski (2003) *J. Comp. Phys. Vol.192:355-364.*

- If A is the area of 2D domain occupied by the fluid (in Ω_2)within the computational cells then, at time $t = t^n$ the area of the fluid, f, in Ω_2 in each of the cells can be written as
$$F^n_{f,i,j} A_{i,j}$$
- Geometrically, the conservation of mass in this domain means that the total area at each time step is conserved so that $\sum_{i,j} F^{n+1}_{f,i,j} A_{i,j} = \sum_{i,j} F^n_{f,i,j} A_{i,j}$.
- This advection equation is satisfied explicitly by introducing linear mappings, Π_x and Π_y, in both coordinate directions. The combination of two linear mappings $\Pi_{xy} = \Pi_x + \Pi_y$ is used to transform the fluid region at time $t = t^n$ into the fluid region at time $t = t^{n+1}$.

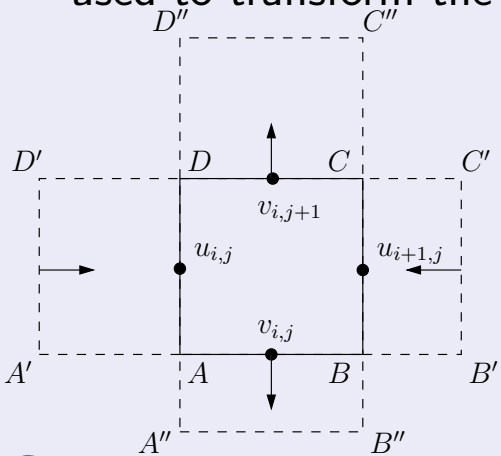

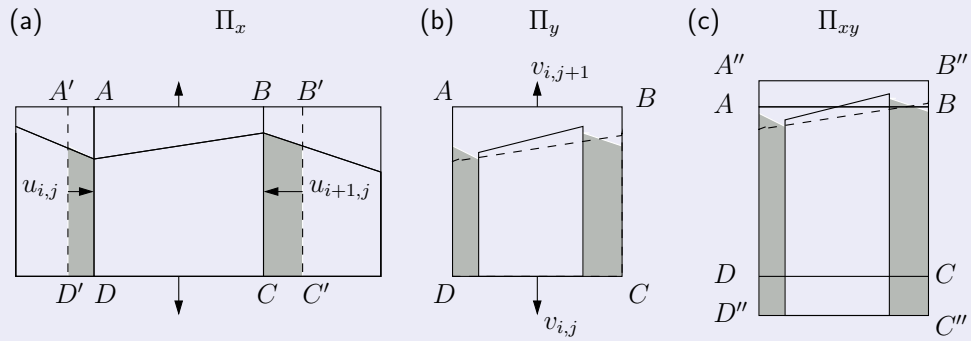

1. Fluid polygons located in the rectangle $A'B'C'D'$ are identified.
2. Linear mapping along the x-direction maps (compresses) $A'B'C'D'$ onto $ABCD$
3. Linear mapping along the y-direction maps (expands) $ABCD$ onto $A''B''C''D''$

Total volume of the fluid in $p(i,j)$ is calculated at $t = t^{n+1}$ as a sum of all fluid contributions from four neighbour cells (left, right, top, bottom) as well as the cell $p(i,j)$ itself.

Method

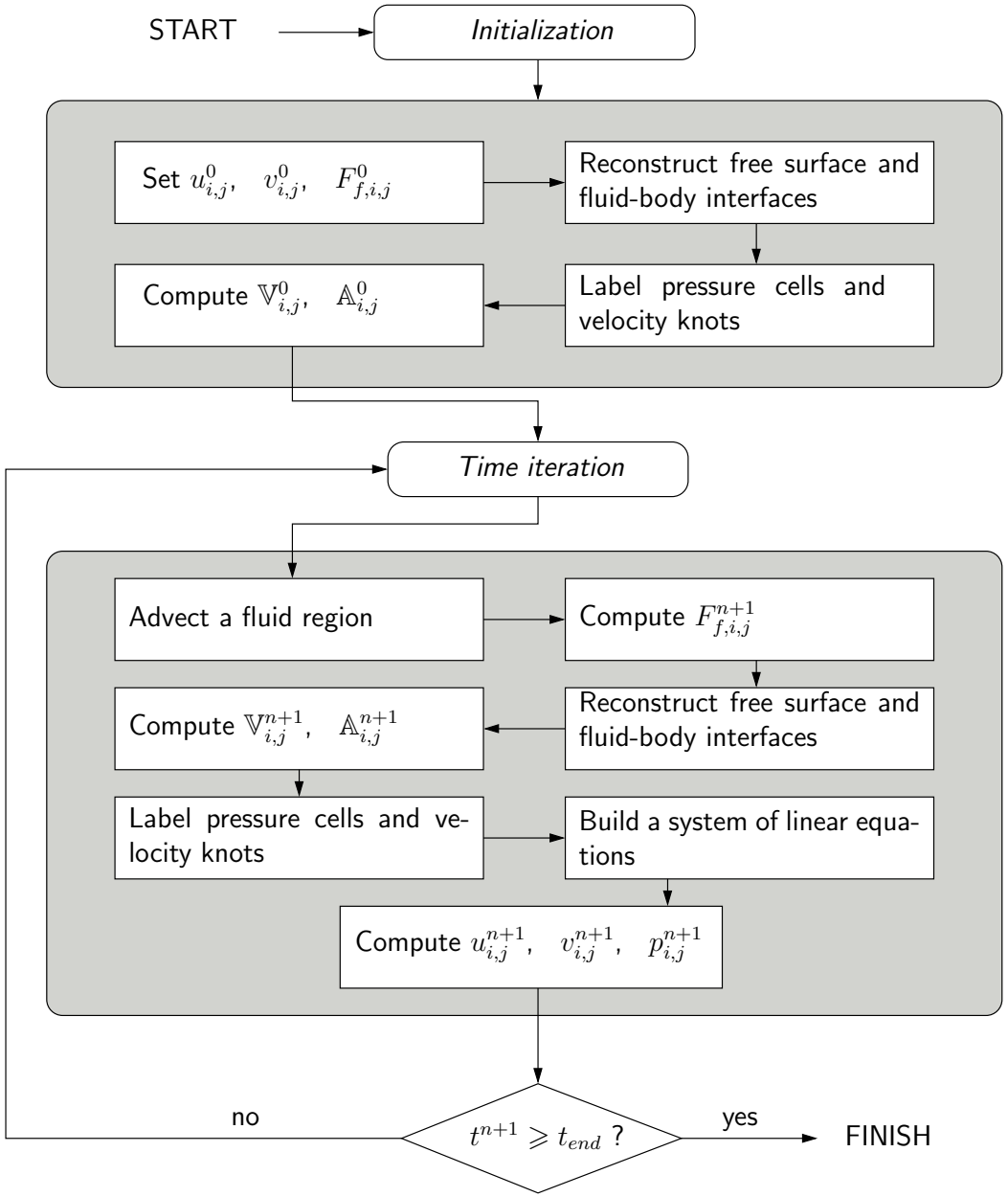
START
Initialization
Set $u^0_{i,j}$, $v^0_{i,j}$, $F^0_{f,i,j}$
Reconstruct free surface and fluid-body interfaces
Compute $\mathbb{V}^0_{i,j}$, $\mathbb{A}^0_{i,j}$
Label pressure cells and velocity knots
Time iteration
Advect a fluid region
Compute $F^{n+1}_{f,i,j}$
Compute $\mathbb{V}^{n+1}_{i,j}$, $\mathbb{A}^{n+1}_{i,j}$
Reconstruct free surface and fluid-body interfaces
Label pressure cells and velocity knots
Build a system of linear equations
Compute $u^{n+1}_{i,j}$, $v^{n+1}_{i,j}$, $p^{n+1}_{i,j}$
$t^{n+1} \geqslant t_{end}$?
no
yes
FINISH

◀ Method

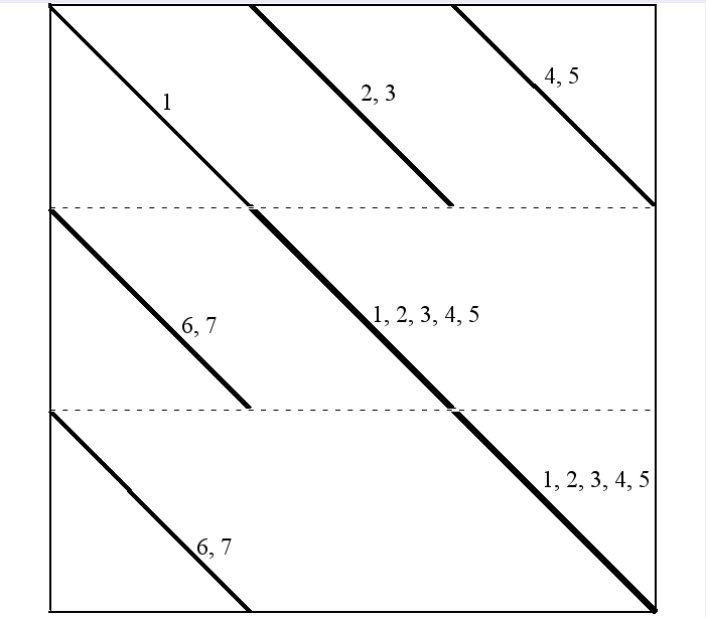

- Matrix is sparse with size $3 \times N \times M$

  N and M: number of knots along x- and y-axes

  e.g. $N = 200$ and $M = 160$: $3 \times N \times M = 96000$

- GMRES method with ILUT preconditioner is used
- Trilinos library is used
- Simulations up to $t = 100$ require about 504 hours

Upper block: Built of the discrete continuity equations added for $p_{i,j}$

- Non-zero elements in line "1": $p_{i,j}$ located in the cylinder/at the domain boundary
- Lines "2": $u_{i,j}$; "3": $u_{i+1,j}$; "4": $v_{i,j}$; "5": $v_{i,j+1}$

Middle block: Built of the discrete momentum equations added for $u_{i,j}$

- Lines "1": $u_{i,j}$; "2": $u_{i-1,j}$; "3": $u_{i+1,j}$; "4": $u_{i,j-1}$; "5": $u_{i,j+1}$
- Lines "6": $p_{i-1,j}$; "7": $p_{i,j}$

Lower block: Built of the discrete momentum equations added for $v_{i,j}$

- Lines "1": $v_{i,j}$; "2": $v_{i-1,j}$; "3": $v_{i+1,j}$; "4": $v_{i,j-1}$; "5": $v_{i,j+1}$
- Lines "6": $p_{i,j-1}$; "7": $p_{i,j}$

◀ Method ▶▶ computational mesh

Computational mesh

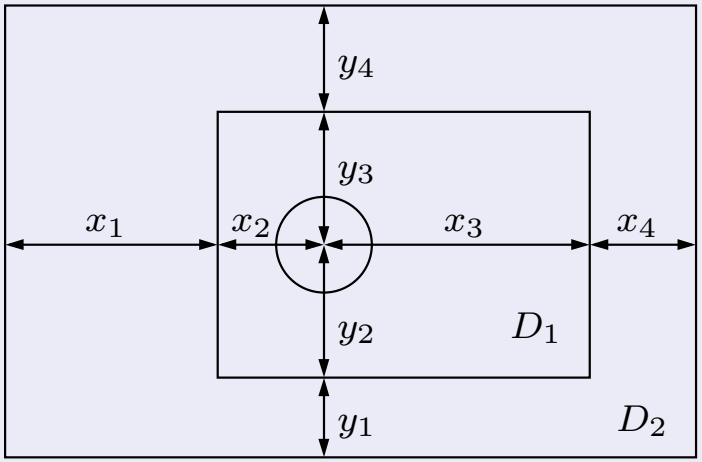

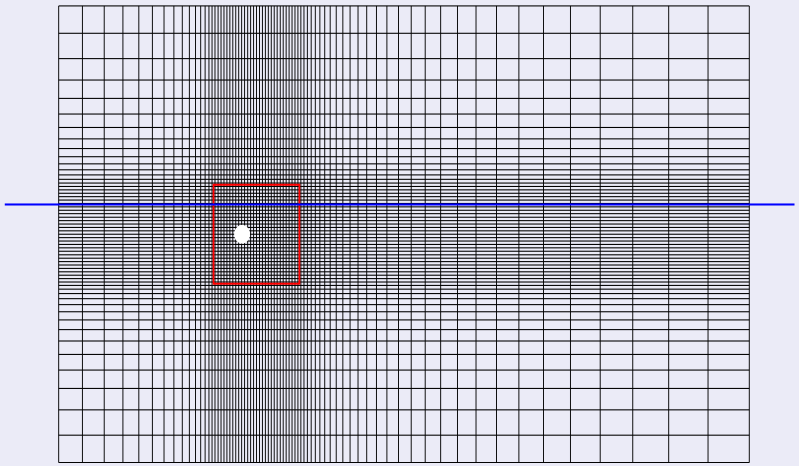

- D_1 region: uniform fine grid; D_2 region: exponentially expanding grid
- Exponential distribution of N knots, $\{x_i\}_{i=1}^{N}$, in $[x_a, x_b]$:

  $x_i = x_a + (x_b - x_a)\frac{e^{a\varsigma_i}-1}{e^a-1}, \qquad \varsigma_i = \frac{i-1}{N-1}, \qquad i = 1, \ldots, N$

  ς_i: uniform distribution of N knots in the interval $[0, 1]$
- a: computed from $f(a) = \Delta h - (x_b - x_a)\frac{e^{a/(N-1)}-1}{e^a-1}$ using Brent's algorithm (1973) ▸▸ B
- a: chosen so that the first grid step of the exponential grid in the grids overlap region equals to the uniform grid step, Δh

Typical numerical parameters

	x_1	x_2	x_3	x_4	y_1	y_2	y_3	y_4
Length	$17d$	$3d$	$7d$	$23d$	$16d$	$4d$	$4d$	$16d$
Number of knots	20	30	80	50	20	42	42	20

- Flow past a stationary cylinder in the absence of a free surface at $R = 200$ is solved to evaluate the spatial and temporal accuracies of the method
- The near wake grid resolution is examined by using three different grids with $40, 60, 90$ cells per cylinder diameter. The time step $\Delta t = 0.005$ is chosen for the grid resolution test
- The sensitivity of the accuracy of computations to the value of the time step is tested using the same grid (60 cells per cylinder diameter) for three different values of the time step, $\Delta t = 0.005, 0.0075, 0.01$

Parameter	Grid cells per cylinder diameter			Δt		
Value	40	60	90	0.01	0.0075	0.005
f_0	0.194	0.194	0.195	0.194	0.195	0.196
$C_{L,max}$	0.659	0.663	0.673	0.668	0.669	0.671
$\widehat{C_D}$	1.297	1.300	1.319	1.305	1.307	1.311

The effects of the near wake grid resolution and the time step, Δt, on the maximum lift coefficient, $C_{L,max}$; the mean drag coefficient, $\widehat{C_D}$; the natural vortex shedding frequency, f_0, for the case of uniform flow past a stationary cylinder in the absence of a free surface at $R = 200$.

- Increase in the number of cells per cylinder diameter from 60 to 90 has a negligible effect on the computed quantities.
- The grid resolution of 60 cells per diameter and $\Delta t = 0.0075$ found to be sufficient to capture the physical development of the flow in the boundary layer region accurately.

Uniform flow past a streamwise oscillating cylinder in the absence of a free surface

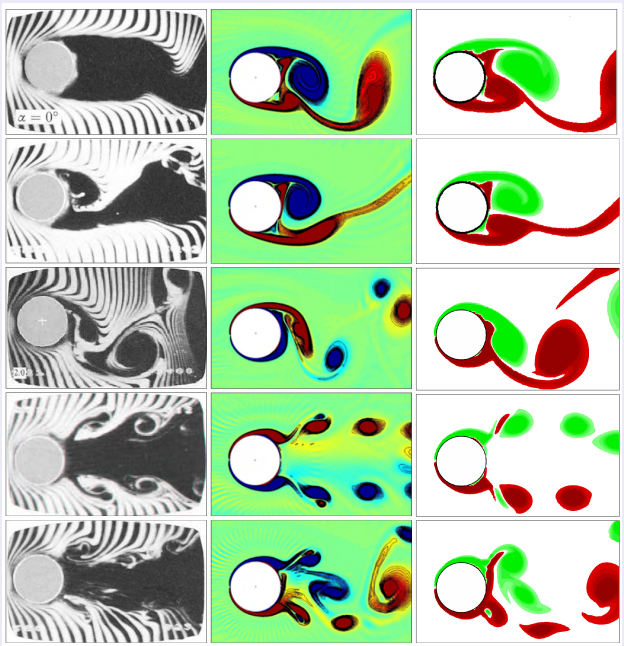

The equivorticity lines at $R = 855$: $A = 0.13$ (from top to bottom: $f/f_0 = 0.5$, 1.0, 2.0, 3.0, 4.0): experimental results of Ongoren and Rockwell (1988), *J. Fluid Mech., Vol.191:225-245* (left); numerical results of Al-Mdallal (2004), *Ph.D. thesis, Memorial Univ.* (middle); present results (right).

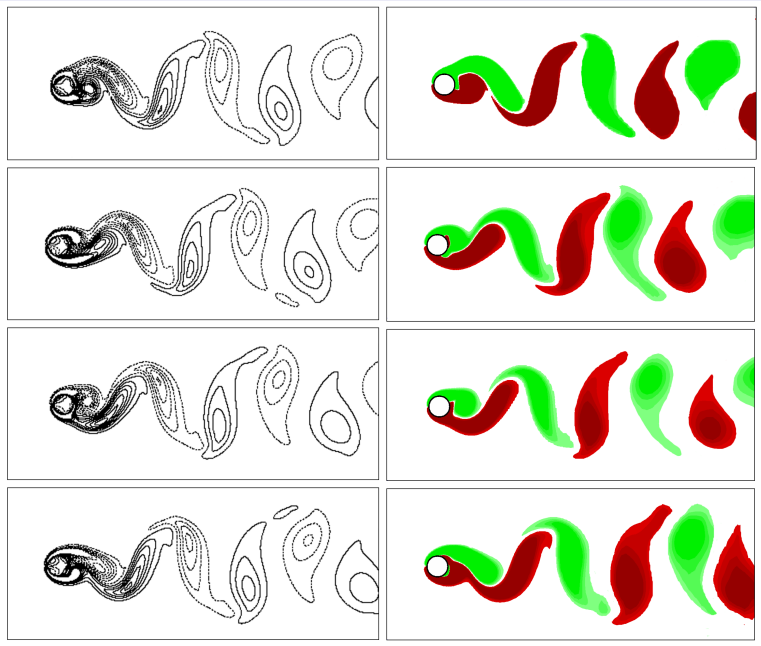

The equivorticity lines at $R = 100$: $A = 0.14$, $f/f_0 = 2$ (from top to bottom: $t/T_0 = 1/4$, $1/2$, $3/4$, 1.0 ($T_0 = 5.91$)): numerical results of Su, Lai and Lin (2007), *Comp. Fluids, Vol.36:313-324* (left); present results (right).

Reference	Present	Su, Lai and Lin (2007)	Hurlbut, Spaulding and White (1982)
$C_{L,max}$	0.92	0.97	0.95
$\widehat{C_D}$	1.70	1.70	1.68

The comparison of the maximum lift coefficient, $C_{L,max}$ and the mean drag coefficient, $\widehat{C_D}$, at $R = 100$: $A = 0.14$, $f/f_0 = 2.0$ with the numerical results of Su, Lai and Lin (2007) and Hurlbut, Spaulding and White (1982), *J. Fluids Eng., Vol.104:214-222*.

Uniform flow past a stationary cylinder in the presence of a free surface at $R = 180$

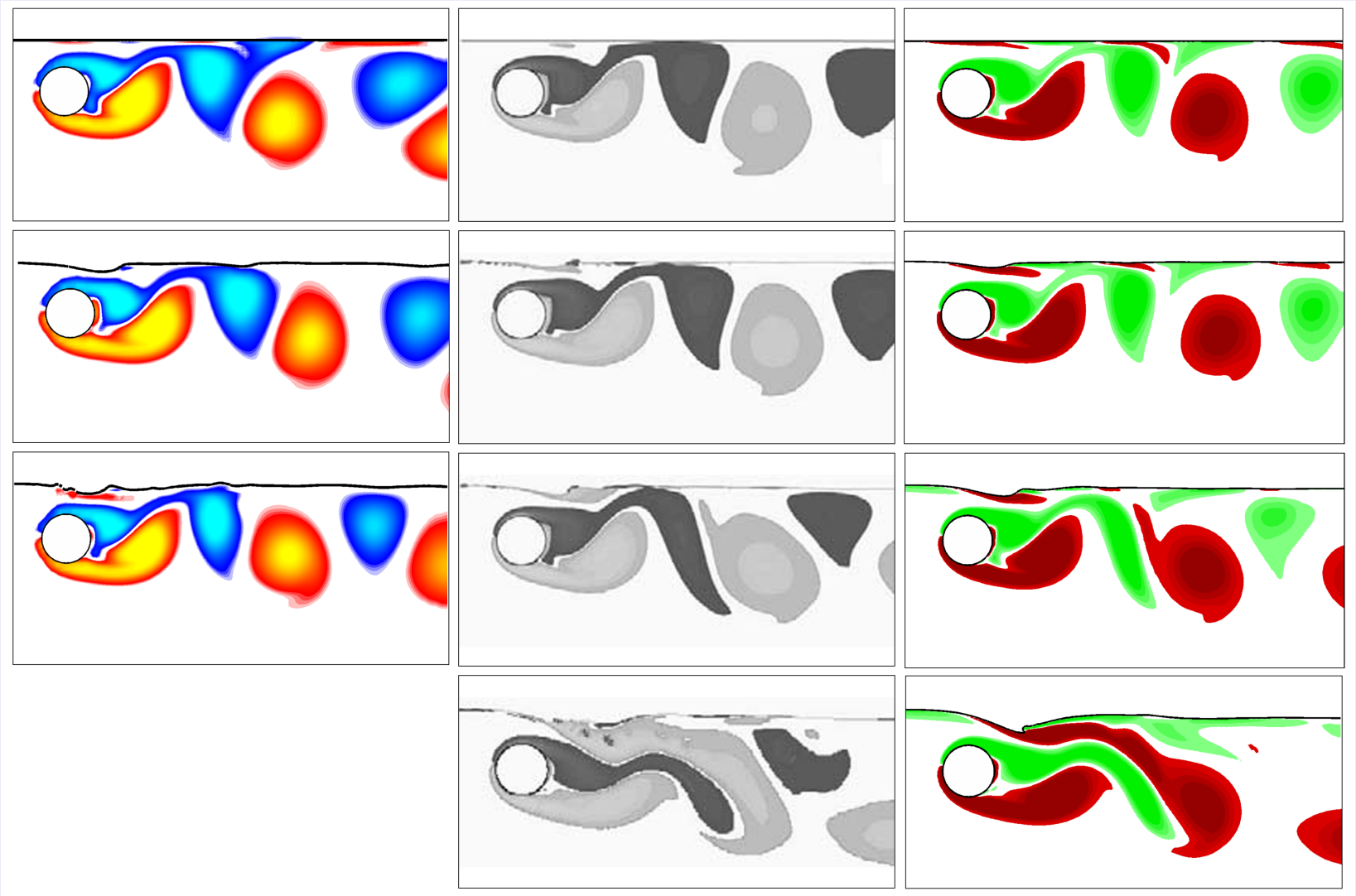

The equivorticity patterns and the free surface deformations for $h = 0.55$: $Fr = 0, 0.3, 0.4, 0.6$ (from top to bottom). Gubanov (2006) *MSc thesis, Memorial University* (left), Reichl, Hourigan and Thompson (2005), *J. Fluid Mech., Vol.533:269-296* (middle), present (right).

The effect of the free surface inclusion at $Fr = 0.4$, $h = 0.5$ on vortex shedding modes and their periods, T_v ("*": quasi-locked-on modes)

	$Fr = 0.4, h = 0.5$		$h = \infty$	
f/f_0	Mode	T_ν	Mode	T_ν
1.5	**4S*** $(T \le t \le 20T)$; non-locked $(21T \le t \le 29T)$	3T -	**2P**	2T
2.5	**C(6S)*** $(5T \le t \le 33T)$; non-locked $(34T \le t \le 49T)$	7T -	**C(6S)***	8T
3.5	**C(4S)***$(7T \le t \le 40T)$; non-locked $(41T \le t \le 68T)$	7T -	**C(2S)***(within $71T$) non-locked $(72T \le t \le 104T)$	4T -

- For each f/f_0, a transition occurs from quasi-periodic state to non-periodic state.
- The vorticity layers origination from the free surface and the upper surface of the cylinder are central determining the wake states.
- The coalescence between the vortices occurs $f/f_0 = 2.5, 3.5$.
- A switchover in the vortex shedding modes is observed as h decreases.

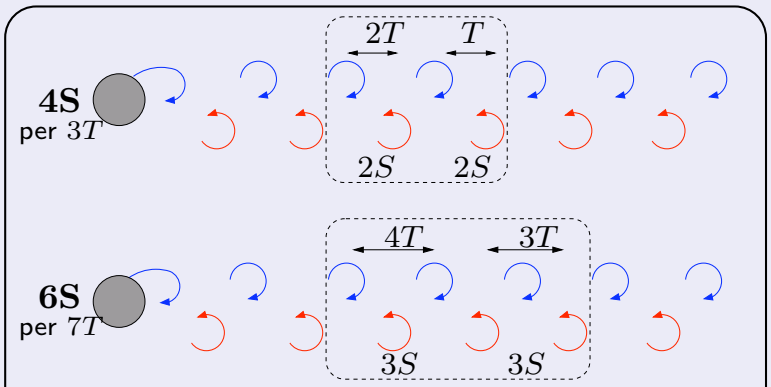

New vortex shedding modes:

- **4S**: four single vortices are shed per $T_v(= 3T)$ for $f/f_0 = 1.5, 3.5$
- **6S**: six single vortices are shed per $T_v(= 7T)$ for $f/f_0 = 2.5$

The equivorticity patterns (left) and the pressure contours (right) over $3T$, at $R = 200$: $A = 0.13, f/f_0 = 1.5, Fr = 0.4, h = 0.5$ $(26.94 \leq t \leq 37.04)$ i.e., $(8T, 11T)$ $(T \approx 3.367)$.

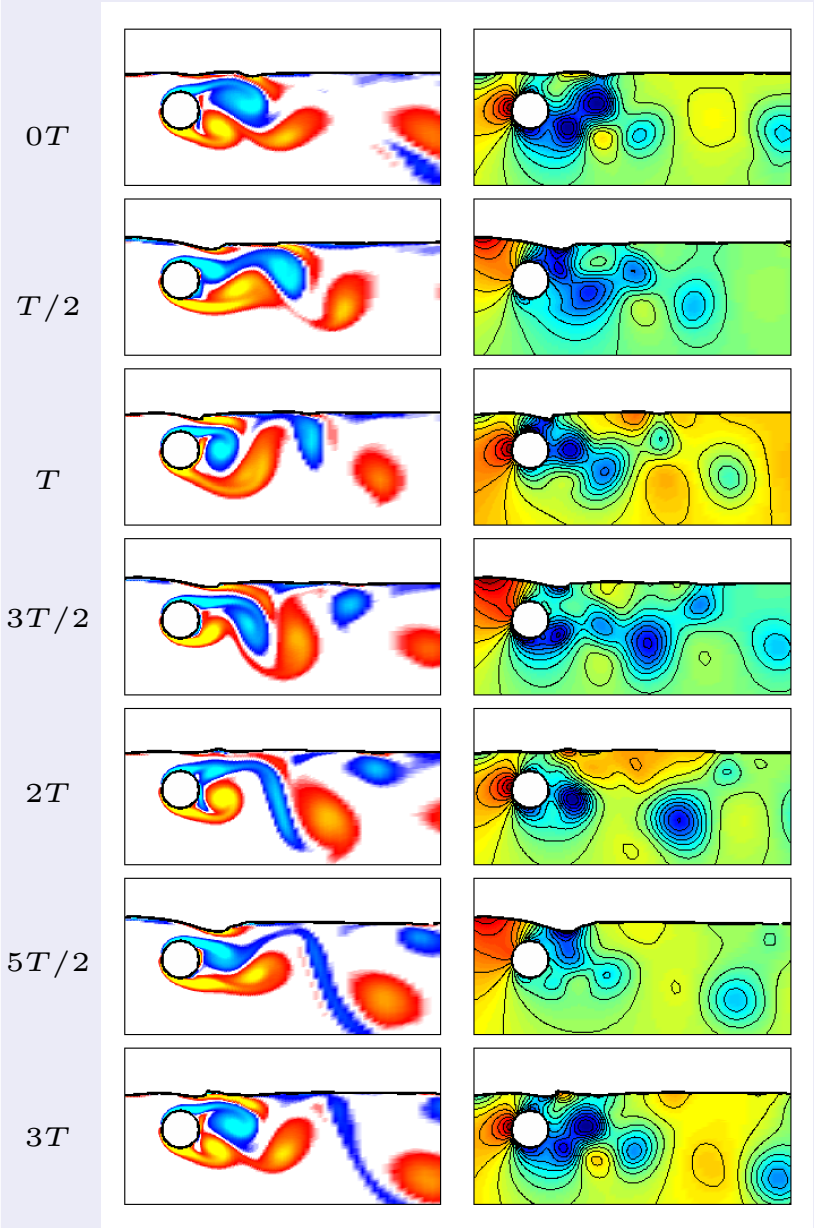

- The vortex shedding mode is quasi-locked-on **4S** mode, per $3T$ (within $20T$): four single vortices are shed per $3T$.
- Positive and negative vortices developed in the previous vortex shedding cycle are shed at $t \approx T/2$ and $t \approx T$, respectively.
- The positive vortex developed over $0T \leq t \leq 3T/2$ attaches to the positive vortex from the free surface, and envelops the negative vortex in the upper vortex shedding layer.
- These vortices are shed from the lower and upper part of the cylinder at $t \approx 2T$ and $t \approx 3T$, respectively.
- The highest pressure region seems to switchover between the front of the cylinder and the upper left side of the cylinder.
- The shedding of the negative vortices at $t \approx T$ and $t \approx 3T$ seems to induce a local free surface rising due to the development of sufficiently high pressure region
- At $t = 0T$ the lowest pressure region occurs behind the cylinder and the bottom of the cylinder and then it changes its location to the top of the cylinder at $t = 5T/2$.

The time variation of the lift coefficient, C_L, and the cylinder displacement, $x(t)$, and Lissajous patterns of C_L at $R = 200$: $A = 0.13$, $f/f_0 = 1.5$, $Fr = 0.4$

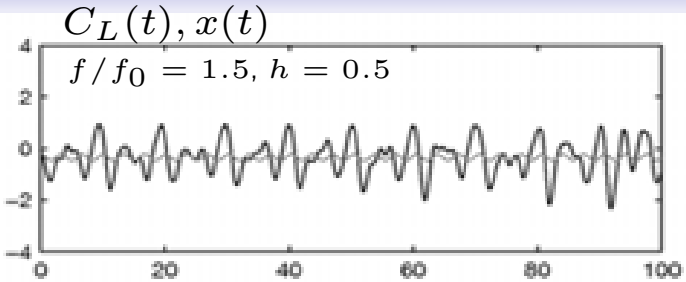

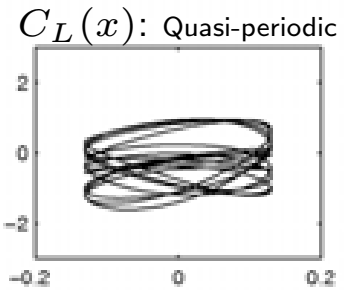

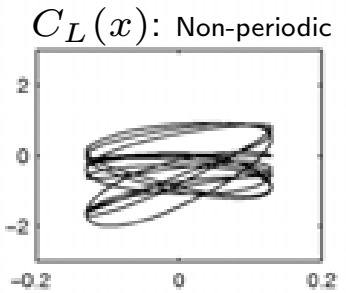

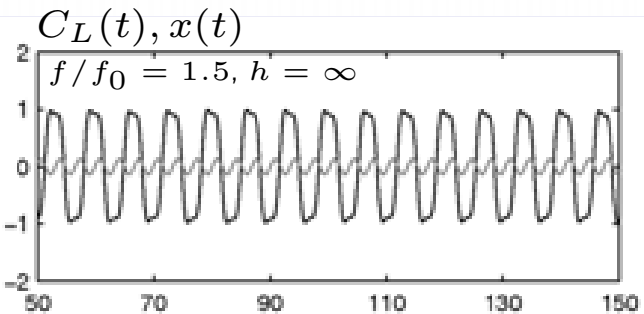

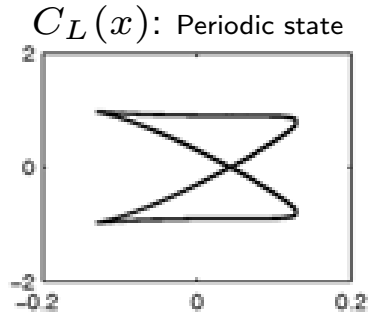

In the presence of a free surface:

- The transition of the flow regime from the quasi-periodic state into the non-periodic state is observed.
- The traces of the lift coefficient are almost periodic over $3T$ within first $20T$, and then they become non-persistent when the switching time is reached at approximately $t = 67.34$.
- The Lissajous trajectories of C_L shows that there is a loss of phase-locking. This confirms that the fluctuating lift coefficient is quasi-phase-locked to the cylinder motion in the quasi-periodic state.

In the absence of a free surface:

- The traces of C_L show repeatable patterns over $2T$. This observation is also suggested by the corresponding Lissajous patterns which indicates lock-on between the cylinder motion and the fluctuating C_L.

- The hystresis loops are mostly confined in the lower half plane at $h = 0.5$, which shows that the presence of the free surface breaks the symmetry observed in the case when $h = \infty$.

The link between the changes in the wake dynamics of the cylinder and the lift coefficient, C_L: $R = 200$, $A = 0.13$, $f/f_0 = 2.5$, $Fr = 0.4$ at $h = 0.25,\ 0.5,\ 0.75$.

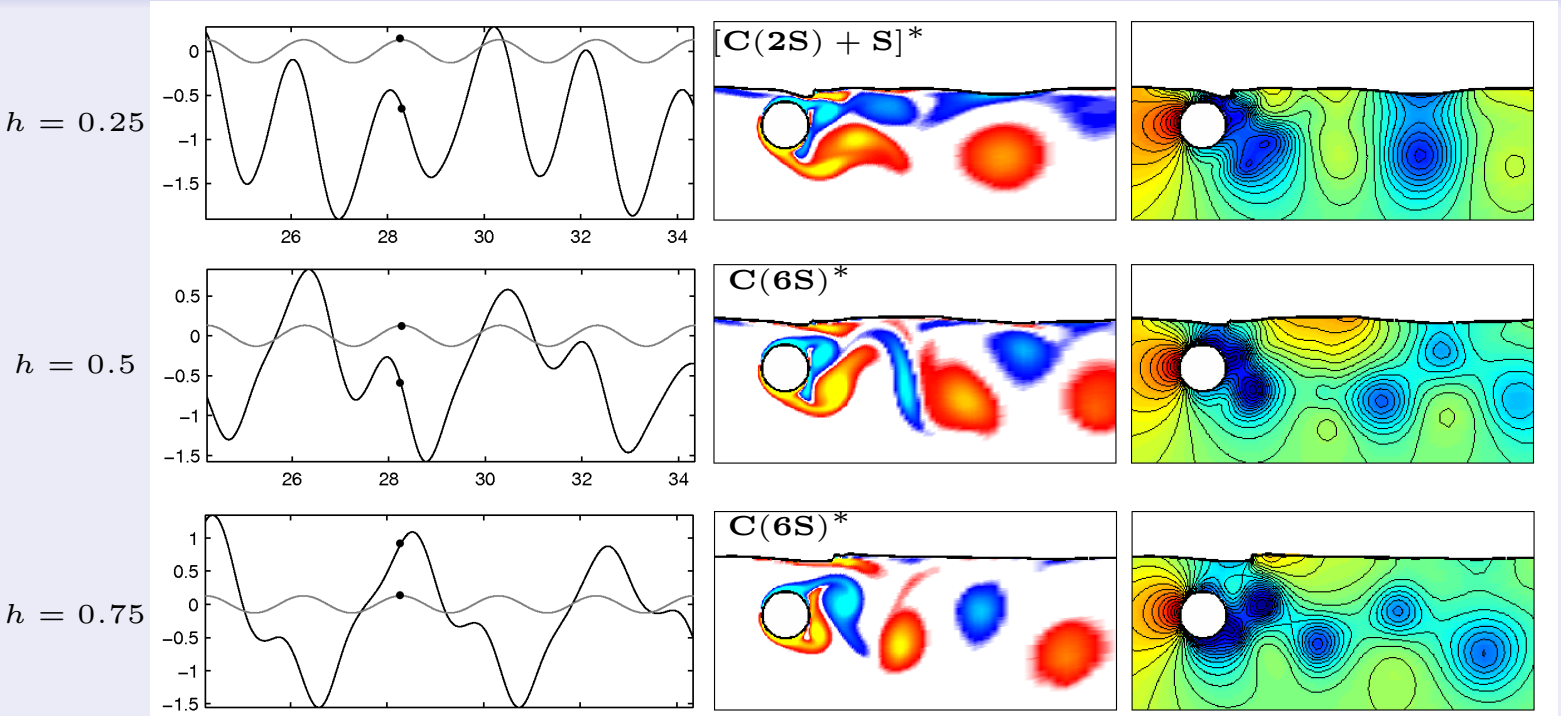

- At $h = 0.25$: C_L displays almost a sinusoidal trace during the development of $\mathbf{C(2S) + S}$ mode whereas two peaks per $2T$ develop on the lift traces with an increase in h during the development of $\mathbf{C(6S)}$ modes.
- C_L indicates almost similar patterns per $2T$ at $h = 0.5$ and $h = 0.75$ with a phase shift, which is confirmed by the corresponding vorticity patterns and pressure contours which are are almost the mirror images of each other due to the mentioned phase shift for C_L, indicating a change in the direction of energy transfer.
- This shift makes a substantial difference in the overall lift behaviour. C_L changes from an extreme negative and positive during the development of $\mathbf{C(2S) + S}$ and $\mathbf{C(6S)}$ modes when $h = 0.25$, $h = 0.75$, respectively.
- The high pressure is associated with the front stagnation point whereas the low pressure concentrates in the lower or upper vortex shedding layers. As the cylinder submergence depth increases from 0.25 to 0.5, the low pressure concentration is mostly shifted from the upper vortex shedding layer to the downstream side of the cylinder. On the other hand, the high pressure remains fixed in the stagnation region for both $h = 0.25$ and $h = 0.5$

- Two-dimensional flow past a circular cylinder subject to forced streamwise oscillations beneath a free surface is investigated based on a two fluid model at $R = 200$, $A = 0.13$, $Fr = 0.4$ for $f/f_0 = 1.5, 2.5, 3.5$ and $h = 0.25$, 0.5, 0.75.
- The inclusion of a free surface seems to stabilize the flow for a short period of time such that the near wake vorticity produces quasi-locked-on modes of vortex shedding and then, the transition of the near wake to the non-periodic state is observed. A similar phenomena has been reported in the experimental study by Cetiner and Rockwell [JFM (2001) **427**:29-59].
- The resulting new modes are the combination of the two and three $\mathbf{2S}$ (or $\mathbf{C(2S)}$) classical modes i.e., $\mathbf{4S}$ (or $\mathbf{C(4S)}$) and $\mathbf{C(6S)}$ modes. In addition, the mode $\mathbf{C(2S) + S}$, which is similar to $\mathbf{C(2S)}$ mode with only one additional vortex shed from the free surface, is observed.
- The lift coefficient changes from an extreme negative during the development of $\mathbf{C(2S) + S}$ shedding when $h = 0.25$ to an extreme positive during the $\mathbf{C(6S)}$ shedding when $h = 0.75$. This substantial difference in the overall lift behaviour is due to a change in the direction of energy transfer.
- The presence of a free surface markedly influences the mean lift force and prolongs the duration of vortex shedding process. These observations suggests that free surface could be used to bring control on the wake structure.
- Irrespective of the values h and f/f_0, the total mechanical energy transfer is negative, indicating the energy transfer from cylinder to fluid unlike the transverse oscillation case.

Acknowledgements

We acknowledge with thanks to Natural Sciences and Engineering Research Council of Canada.

- A special integral form of governing equations (when a solid body is present) is derived by extending the Reynolds transport theorem and then applying it to control volume containing a fluid-body interface

$$\frac{d\mathbb{V}^*}{dt^*} + \int_{\mathbb{A}^*} (\vec{n}\cdot\vec{u}^*)\,\mathrm{d}S^* = 0$$

Derivation summary

$$\frac{d}{dt^*}\int_{\mathbb{V}^*}\vec{u}^*\,\mathrm{d}V^* + \int_{\mathbb{A}^*}(\vec{n}\cdot\vec{u}^*)\vec{u}^*\,\mathrm{d}S^* = -\frac{1}{\rho}\int_{\mathbb{A}^*\cup\mathbb{I}^*} p^*\vec{n}\,\mathrm{d}S^* + \nu\int_{\mathbb{A}^*\cup\mathbb{I}^*}\vec{n}\cdot\nabla\vec{u}^*\,\mathrm{d}S^* + \int_{\mathbb{V}^*}\vec{g}^*\,\mathrm{d}V^*$$

which are valid for a class of viscous flows including free surface flows with arbitrarily moving bodies. Their derivation is based on the theory of generalized functions:

Farassat (1994), *NASA Tech. Rep. 3428*

and the FAVOR technique:

Hirt (1993), *J. Wind Eng. Ind. Aerod.*, Vol.46-47:327-338

1. In FAVOR technique, geometries are embedded in the mesh by setting the area fractions on the control volume faces along with the volume fraction open to flow. This makes the geometry and the grid completely independent of each other, and, as a result, complex solid body can be generated.

Method

2. This technique requires a relatively large number of cells for numerical purposes.

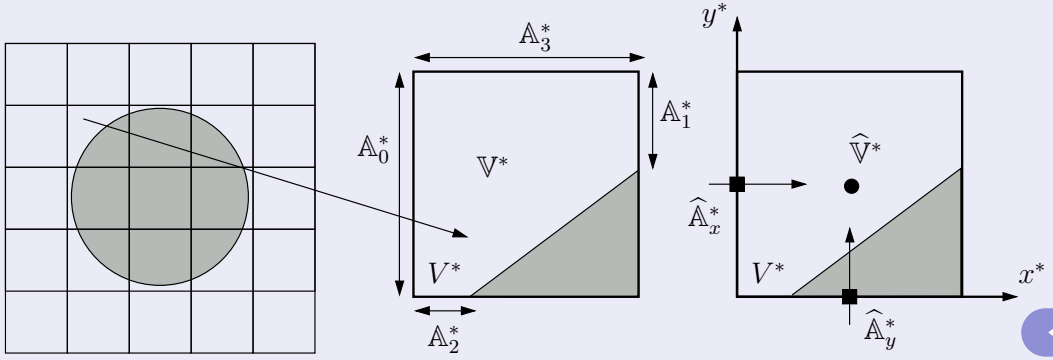

Mathematical model equations

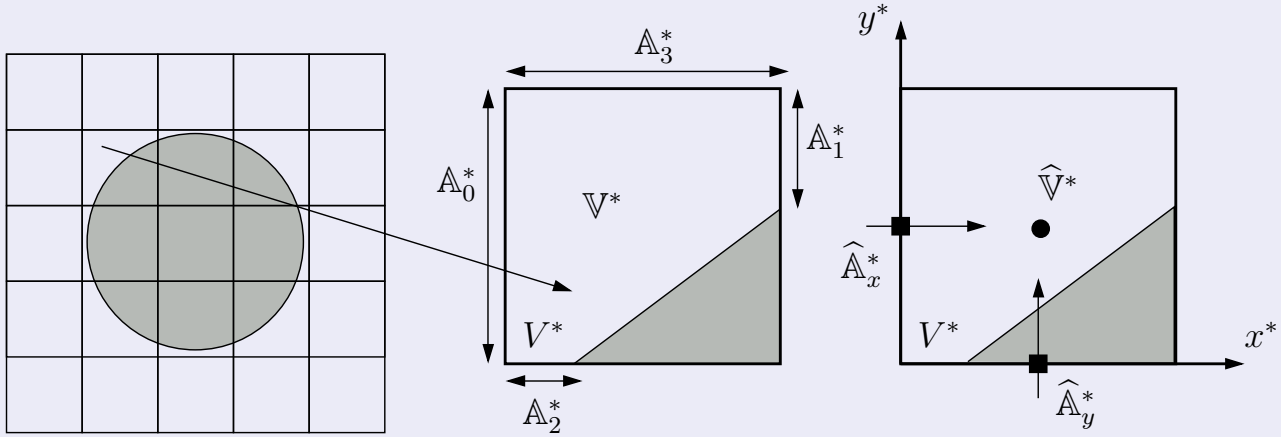

(a) (b) (c)

(a) Typical solid body surface within a Cartesian grid, (b) typical computational cell, V^*, which includes areas, $\mathbb{A}_i^*$ $(i = 0, 1, 2, 3)$ and volume, $\mathbb{V}^*$, open to flow within V^*, (c) location of $\widehat{\mathbb{A}}_x^*$, $\widehat{\mathbb{A}}_y^*$ and $\widehat{\mathbb{V}}^*$ within the computational cell, V^*. The solid body is shown in gray.

- $\widehat{\mathbb{A}}_x^*$, $\widehat{\mathbb{A}}_y^*$ and $\widehat{\mathbb{V}}^*$ are defined as

$$\widehat{\mathbb{V}}^* = \lim_{V^* \to 0} \bar{\mathbb{V}}^*, \qquad \widehat{\mathbb{A}}_x^* = \lim_{S_x^* \to 0} \bar{\mathbb{A}}_x^*, \qquad \widehat{\mathbb{A}}_y^* = \lim_{S_y^* \to 0} \bar{\mathbb{A}}_y^*$$

$$\bar{\mathbb{V}}^* = \frac{1}{V^*} \int_{V^*} H \, dV^*, \qquad \bar{\mathbb{A}}_x^* = \frac{1}{S_x^*} \int_{S_x^*} H \, dS^*, \qquad \bar{\mathbb{A}}_y^* = \frac{1}{S_y^*} \int_{S_y^*} H \, dS^*$$

$H(\vec{x}^*)$ is the Heaviside function that is equal to unity in the fluid region and zero in the solid body.

- Special integral form of governing equations can be obtained from the differential form of FAVOR equations using

$$\int_{V^*} \widehat{\mathbb{V}}^* \, dV^* = \frac{\mathbb{V}^*}{V^*}, \qquad \int_{S^*} \widehat{\mathbb{A}}_x^* \, dS^* = \frac{\mathbb{A}_0^*}{S_0^*}, \qquad \int_{S^*} \widehat{\mathbb{A}}_y^* \, dS^* = \frac{\mathbb{A}_2^*}{S_2^*}.$$

- Traditional approaches consider the integral form of the governing equations over control volumes containing only fluid. In this work, special integral form of the governing equations over control volumes containing a fluid-solid interface.

Differential form of FAVOR equations:

$$\frac{\partial \widehat{\mathbb{V}}^*}{\partial t^*} + \frac{\partial (u^* \widehat{\mathbb{A}}_x^*)}{\partial x^*} + \frac{\partial (v^* \widehat{\mathbb{A}}_y^*)}{\partial y^*} = 0$$

$$\frac{\partial u^*}{\partial t^*} + \frac{1}{\widehat{\mathbb{V}}^*}\left(u^* \widehat{\mathbb{A}}_x^* \frac{\partial u^*}{\partial x^*} + v^* \widehat{\mathbb{A}}_y^* \frac{\partial u^*}{\partial y^*}\right) = F_1^* - \frac{1}{\rho}\frac{\partial p^*}{\partial x^*} + \nu \nabla^2 u^*$$

$$\frac{\partial v^*}{\partial t^*} + \frac{1}{\widehat{\mathbb{V}}^*}\left(u^* \widehat{\mathbb{A}}_x^* \frac{\partial v^*}{\partial x^*} + v^* \widehat{\mathbb{A}}_y^* \frac{\partial v^*}{\partial y^*}\right) = F_2{}^* - \frac{1}{\rho}\frac{\partial p^*}{\partial y^*} + \nu \nabla^2 v^*$$

Integral form of FAVOR equations:

$$\frac{d\mathbb{V}^*}{dt^*} + \int_{\mathbb{A}^*} (\vec{n} \cdot \vec{u}^*)\, \mathrm{d}S^* = 0$$

$$\frac{d}{dt^*} \int_{\mathbb{V}^*} \vec{u}^*\, \mathrm{d}V^* + \int_{\mathbb{A}^*} (\vec{n} \cdot \vec{u}^*)\vec{u}^*\, \mathrm{d}S^*$$

$$= -\frac{1}{\rho} \int_{\mathbb{A}^* \cup \mathbb{I}^*} p^* \vec{n}\, \mathrm{d}S^* + \nu \int_{\mathbb{A}^* \cup \mathbb{I}^*} \vec{n} \cdot \nabla \vec{u}^*\, \mathrm{d}S^* + \int_{\mathbb{V}^*} \vec{F}^*\, \mathrm{d}V^*$$

$\widehat{\mathbb{V}}^* = \lim_{V^* \to 0} \frac{1}{V^*} \int_{V^*} H\, dV^*$ $\quad$ $\widehat{\mathbb{A}}_i^* = \lim_{S_i^* \to 0} \frac{1}{S_i^*} \int_{S_i^*} H_i\, dS^*,\ i = x, y$

Generalized transport theorem

and the FAVOR method

Hirt and Sicilian's porosity equations:

$$\frac{\partial H}{\partial t^*} + \nabla \cdot (H \vec{u}^*) = 0$$

$$\frac{\partial (H \vec{u}^*)}{\partial t^*} + \nabla \cdot (H \vec{u}^* \vec{u}^*) = -\frac{1}{\rho} H \nabla p^* + \nu \nabla \cdot H \nabla \vec{u}^* + H \vec{F}^*$$

Multiplication by the Heaviside function, H

Differential form of continuity and momentum equations:

$$\frac{\partial \rho}{\partial t^*} + \nabla \cdot \rho \vec{u}^* = 0$$

$$\frac{\partial \rho \vec{u}^*}{\partial t^*} + (\rho \vec{u}^* \cdot \nabla)\, \vec{u}^* = -\nabla p^* + \mu \nabla^2 \vec{u}^* + \rho \vec{F}^*$$

Integral form of continuity and momentum equations:

$$\frac{d}{dt^*} \int_{V^*(t^*)} \rho\, \mathrm{d}V^* = 0$$

$$\frac{d}{dt^*} \int_{V^*(t^*)} \rho \vec{u}^*\, \mathrm{d}V^* = \int_{V^*(t^*)} \rho \vec{F}^*\, \mathrm{d}V^* + \int_{\partial V^*(t^*)} \bar{\bar{\sigma}} \cdot \vec{n}\, \mathrm{d}S^*$$

The derivation of the differential and integral forms of the FAVOR equations: (Hirt (1993), J. Wind Eng. Ind. Aerod., Vol.46-47:327-338 (left) and present work (right).

◀ Mathematical model

Points used to approximate $\dfrac{\partial u}{\partial x}$ are constructed differently in each of the two possible situations:

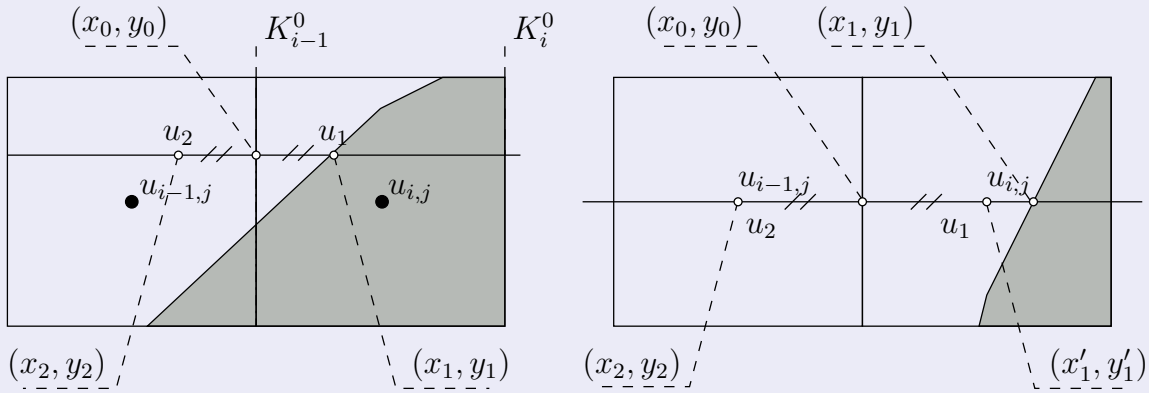

(a) (b)

Situation (a):

1. Reconstruct the line parallel to the x-axis which passes through the point (x_0, y_0)
2. If $x_1 - x_0 \leqslant \dfrac{K^0_i - K^0_{i-1}}{2}$, then (x_1, y_1) is reflected into (x_2, y_2)
3. $u(x_2, y_2)$: B-spline interpolation; $u(x_1, y_1)$: no-slip condition; $\left.\dfrac{\partial u}{\partial x}\right|_{(x_0,y_0)} \approx \dfrac{u_1 - u_2}{x_1 - x_2}$
4. No line intersection or $x_1 - x_0 > \dfrac{K^0_i - K^0_{i-1}}{2}$: points located at $x_1 - x_0$ from (x_0, y_0) are used

Situation (b):

1. Points (x'_1, y'_1) and (x_2, y_2) are used for the derivative approximation

$$\frac{d}{dt}\int_{\mathbb{V}} u \, \mathrm{d}V + \int_{\mathbb{A}} (\vec{n}\cdot\vec{u})u \, \mathrm{d}S = -\frac{1}{\varepsilon}\int_{\mathbb{A}\cup\mathbb{I}} pn_1 \, dS + \frac{1}{R}\int_{\mathbb{A}\cup\mathbb{I}} \vec{n}\cdot\nabla u \, dS + \int_{\mathbb{V}} F_1 \, dV$$

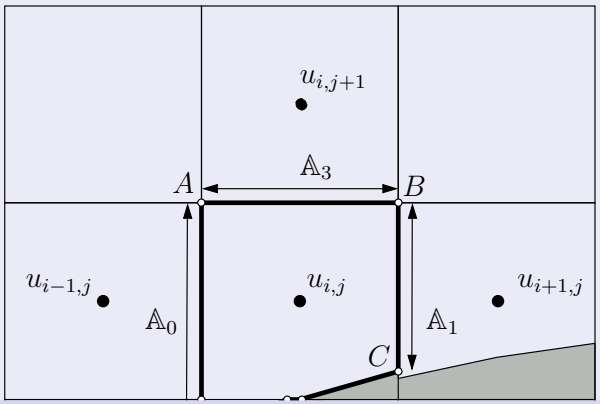

- **FF** cell borders **FF**, **DF** or **DD** cell.
  Velocities and their normal derivatives at the edges of velocity cells are approximated using a linear interpolation between fluid neighbour velocity knots (standard discretization).
- **FF** cell borders **BF** cell (neighbour velocity may be located in the region occupied by the solid body).
  1. Cell merging procedure is used.

The resulting linear equation

$$C_0 u_{i,j}^{n+1} + C_1 u_{i-1,j}^{n+1} + C_2 u_{i+1,j}^{n+1} + C_3 u_{i,j-1}^{n+1} + C_4 u_{i,j+1}^{n+1} + C_5 p_{i-1,j}^{n+1} + C_7 p_{i,j}^{n+1} = C_8$$

Method

- Many studies exclude **BF** cells from consideration and apply the no-slip condition to calculate **BF**-velocity.
- In this work, the cell merging technique is used to discretize the Navier-Stokes equations in such **FF** cells to ensure that global second-order accuracy is preserved.

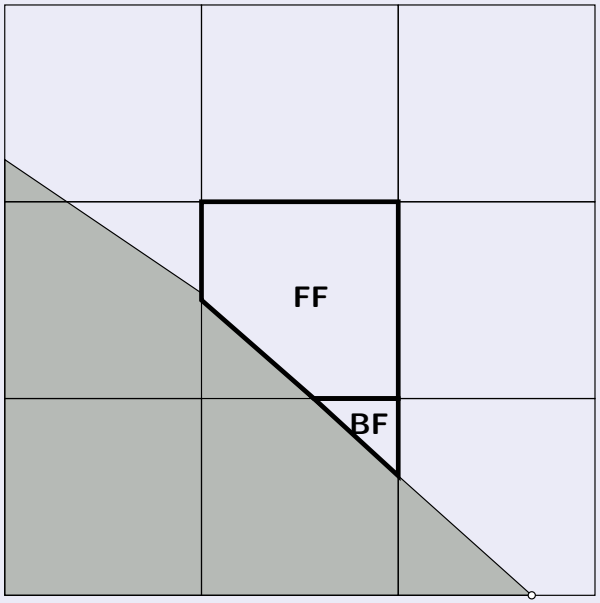

- **BF** cell can border more than one **FF** cell
- For such **BF** cell, the master cell is chosen to be the neighbour **FF** cell with the largest common area aperture
- Choice of master cells guarantees that the slave cell may have only one master cell
- Each master cell can have from one to four slave cells

- **FF** is the master cell for neighbouring **BF** cell
- Slave cell becomes attached to this master cell
- This results in the reshaping of the master cell
- Depending on the location and the local orientation of the fluid-body interface, cells of a wide variety of shapes can be formed

◂ Discr. N-S. eq

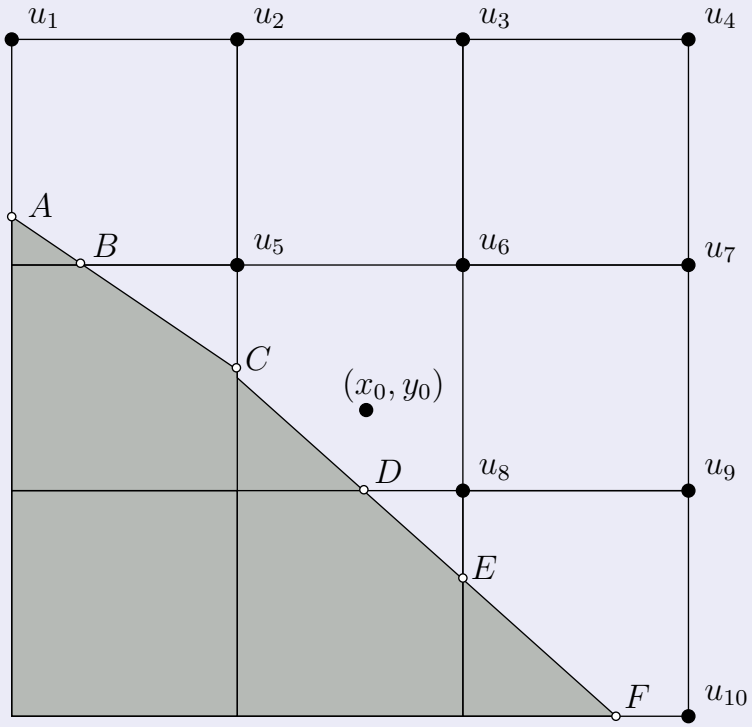

- Let (x_0, y_0) be the point at which the u-velocity must be interpolated
- Consider a 3×3 block of the neighbouring cells
- Points of intersection of the grid with the fluid-body interface (A to F) are used to define the locations of the fluid-body interface velocities

- Values of velocities at the points of intersection are calculated using the no-slip boundary condition (set to the velocities of the cylinder calculated at points $A, \ldots, F$)
- Interface velocities and the neighbouring **FF** velocities ($u_1, \ldots, u_{10}$ in an example case) are calculated at time $t = t^n$
- These velocities are used to reconstruct the B-spline surface
- Finally, the value of the u-velocity in the point (x_0, y_0) can be calculated

◂ Discr. N-S. eq

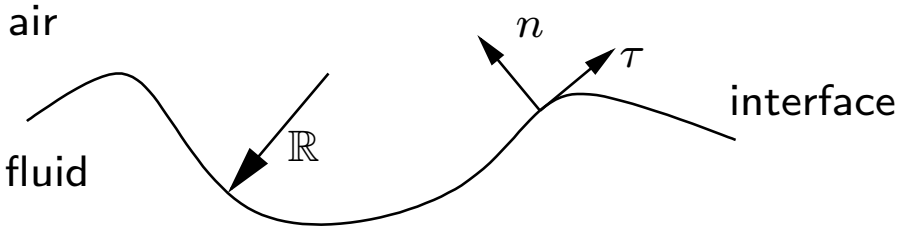

- Free surface represents interface between the air and the fluid
- Interface stress balance condition is
  $stress_{air} + stress_{fluid} + stress_{interface} = 0$

- For incompressible Newtonian fluid

$$Stress_i = -p^* \delta_{ij} \vec{n}_j + \mu \left(\frac{\partial \vec{u}_j^*}{\partial \vec{x}_i^*} + \frac{\partial \vec{u}_i^*}{\partial \vec{x}_j^*} \right) \vec{n}_j \qquad Stress_{interface} = \sigma \left(\frac{1}{\mathbb{R}} \right) (-\vec{n}_i) + \nabla \sigma_i,$$

δ_{ij}: Kronecker delta, σ: surface tension, $\mathbb{R}$: radii of curvature

- $\rho_{fluid} \gg \rho_{air} \Rightarrow p^*_{air} = const$
- In Cartesian coordinates stress balance conditions can be written as

$$2\mu \left(n_1 n_1 \frac{\partial u^*}{\partial x^*} + n_1 n_2 \left(\frac{\partial u^*}{\partial y^*} + \frac{\partial v^*}{\partial x^*} \right) + n_2 n_2 \frac{\partial v^*}{\partial y^*} \right) = p^* - p^*_{air} + \frac{\sigma}{\mathbb{R}}$$

$$2 n_1 \tau_1 \frac{\partial u^*}{\partial x^*} + (n_1 \tau_2 + n_2 \tau_1) \left(\frac{\partial u^*}{\partial y^*} + \frac{\partial v^*}{\partial x^*} \right) + 2 n_2 \tau_2 \frac{\partial v^*}{\partial y^*} = 0$$